ADVANCES IN ATMOSPHERIC SCIENCES, VOL. 34, JULY 2017, 847–858

• **Original Paper** •

# Autumn Snow Cover Variability over Northern Eurasia and Roles of Atmospheric Circulation

Kunhui YE[†1] and Renguang WU[*2]

[1] *Institute of Space and Earth Information Science, The Chinese University of Hong Kong, Hong Kong, China*

[2] *Center for Monsoon System Research/State Key Laboratory of Numerical Modeling for Atmospheric Sciences and Geophysical Fluid Dynamics, Institute of Atmospheric Physics, Chinese Academy of Sciences, Beijing* 100029*, China*

(Received 27 November 2016; revised 18 January 2017; accepted 27 February 2017)

ABSTRACT

This study analyzes the variability of northern Eurasian snow cover (SC) in autumn and the impacts of atmospheric circulation changes. The region of large SC variability displays a southward shift from September to November, following the seasonal progression of the transition zones of surface air temperature (SAT). The dominant pattern of SC variability in September and October features a zonal distribution, and that in November displays an obvious west–east contrast. Surface air cooling and snowfall increase are two factors for larger SC. The relative contribution of SAT and snowfall changes to SC, however, varies with the region and depends upon the season. The downward longwave radiation and atmospheric heat advection play important roles in SAT changes. Anomalous convergence of water vapor flux contributes to enhanced snowfall. The changes in downward longwave radiation are associated with those in atmospheric water content and column thickness. Changes in snowfall and the transport of atmospheric moisture determine the atmospheric moisture content in September and October, and the snowfall appears to be a main factor for atmospheric moisture change in November. These results indicate that atmospheric circulation changes play an important role in snow variability over northern Eurasia in autumn. Overall, the coupling between autumn Eurasian snow and atmospheric circulation may not be driven by external forcing.

**Key words**: Autumn Eurasian snow cover, surface air temperature, surface heat fluxes, atmospheric circulation, water vapor transport

**Citation**: Ye. K. H., and R. G. Wu, 2017: autumn snow cover variability over northern Eurasia and roles of atmospheric circulation. *Adv. Atmos. Sci.*, **34**(7), 847–858, doi: 10.1007/s00376-017-6287-z.

## 1. Introduction

Snow is an important component of the climate system over the mid- and high-latitude land areas. Due to its high albedo and low heat conductivity, changes in snow may modulate the surface energy balance and atmospheric circulation (Barnett et al., 1989; Cohen and Rind, 1991; Yasunari et al., 1991). Snowmelt involves changes in soil moisture and surface runoff—a phenomenon referred to as the snow-hydrological effect (Yasunari et al., 1991). The snow-hydrological effect constitutes a delayed impact of snow on surface evaporation, leading to changes in atmospheric circulation and precipitation after snowmelt (Barnett et al., 1989; Yasunari et al., 1991).

Snow change has both local and non-local effects on climate and atmospheric circulation. Local effects are manifested in changes of surface temperature and geopotential height (Cohen and Rind, 1991; Cohen and Entekhabi, 2001; Henderson et al., 2013; Ye et al., 2015). Non-local effects are realized through its modulation of the land–sea thermal contrast and atmospheric circulation pattern. Eurasian snow change has been linked to the Indian summer monsoon variability, with more snow corresponding to a weaker monsoon (Kripalani et al., 1996; Bamzai and Shukla, 1999; Kripalani and Kulkarni, 1999; Fasullo, 2004; Dash et al., 2005). Eurasian and Tibetan Plateau snow change may influence the spring and summer climate over East Asia (Chen and Wu, 2000; Kripalani et al., 2002; Zhang et al., 2004; Wu and Kirtman, 2007; Wu et al., 2009; Zuo et al., 2012). Further examples of non-local effects include downstream wave pattern and temperature changes in the lower atmosphere (Henderson et al., 2013). The altered atmospheric circulation can even induce sea surface temperature (SST) changes (Henderson et al., 2013).

On the other hand, snow variation is influenced by surface conditions, such as temperature, and by atmospheric circulation (e.g., Clark et al., 1999; Vicente-Serrano et al.,

[†] Current affiliation: Institute of Environment, Energy and Sustainability, The Chinese University of Hong Kong, Hong Kong, China

[*] Corresponding author: Renguang WU
Email: renguang@mail.iap.ac.cn

2007; Henderson and Leathers, 2010; Ye and Lau, 2016). Snow variability in winter over Europe has been shown to be associated with North Atlantic Oscillation (NAO)–related temperature advection, with a positive (negative) NAO corresponding to an snow cover (SC) decrease (increase) (Clark et al., 1999; Seager et al., 2010; Kim et al., 2013). The phase change of the NAO has been found to cause snow anomalies in some areas of northern Eurasia (Gutzler and Rosen, 1992; Clark et al., 1999; Morinaga et al., 2003; Popova, 2007). Snow variability in winter over southwestern Asia is associated with atmospheric circulation–related temperature advection (Clark et al., 1999). During the snowmelt season (i.e., spring), Eurasian SC variability is subjected to both temperature advection (Ueda et al., 2003; Iijima et al., 2007) and non-temperature-related processes, such as wind speed and water vapor convergence (Iijima et al., 2007). Ye et al. (2015) showed the effect of atmospheric circulation change on surface warming and snow reduction in the late 1980s over mid- and high-latitude Eurasia.

Numerous studies have examined the correlation between Eurasian snow and large-scale atmospheric circulation patterns. The phase changes of the NAO have been widely found to cause snow anomalies in some areas of northern Eurasia (Gutzler and Rosen, 1992; Clark et al., 1999; Morinaga et al., 2003; Popova, 2007). The phase changes of Eurasian pattern type 1 have also been shown to cause snow anomalies in southwestern Asia (Clark et al., 1999); see more details for the definition of this teleconnection pattern in Barnston and Livezey (1987). On the other hand, the Siberian pattern, identified by Clark et al. (1999), seems to influence the snow conditions throughout the Eurasian sector in its positive phase. In contrast, the negative phase of the Siberian pattern is mostly notable for its impact on the snow conditions in Eastern Europe. The extreme phases of the Siberian High have not been found to exert control on the snow conditions, which may be due to the masking effects from other patterns (Clark et al., 1999).

Many previous studies on snow variability have focused on the winter and spring seasons. The snow variability in autumn is rarely addressed, despite possibly playing a role in the variations of concurrent atmospheric circulation and climate. As autumn is the season when snow falls over mid- and high-latitude Eurasia, snow anomalies in autumn may contribute to those in the subsequent seasons. As such, the fluctuations of snow in autumn may have implications for snow anomalies in subsequent seasons and their impacts. An apparent connection between autumn SC in northern Eurasia and the winter Artic Oscillation (AO)/NAO has highlighted the predictive value of autumn SC over northern Eurasia (Cohen and Entekhabi, 1999, 2001; Saito and Cohen, 2003). This suggests that the climate conditions in large parts of Eurasia and North America may be predictable several months in advance. This correlation has been found to be robust in both observations and model simulations, and the associated physical linkage has been well documented (Saito et al., 2001; Gong et al., 2003, 2004; Allen and Zender, 2011; Cohen et al., 2014). Despite the importance of autumn snow variability in northern Eurasia, its variability and causes have not received much attention. The purpose of this paper is to address the variations of the autumn snow over northern Eurasia and to understand associated changes in surface conditions and atmospheric circulation. Improved knowledge of autumn snow variability in Eurasia may be of help in predicting wintertime climate across the Northern Hemisphere.

This paper is organized as follows: Section 2 describes the data used in this study. Major modes of monthly SC variability in autumn and associated changes in snow water equivalent (SWE) and snow depth (SD) are presented in section 3. In section 4, the surface conditions and surface heat fluxes associated with the major mods of SC variability are analyzed. Section 5 explores the changes in atmospheric circulation and water vapor transport that accompany autumn SC variations. Section 6 summarizes the main findings of this study.

## 2. Data

Northern Hemisphere EASE-Grid (Equal-Area Scalable Earth Grid), version 2.0, weekly SC data, along with version 4 Sea Ice Extent data, from the National Snow and Ice Data Center (NSIDC) (Brodzik and Armstrong, 2013), are used in the present study. This dataset covers the period 1966–2014, and has a spatial resolution of 25 km. For ease of analysis, the original weekly data are converted to monthly data on a regular 1° latitude–longitude grid. The monthly SC defined in this way indicates the time of SC, rather than snow area, within one month. This dataset is most appropriate for large-scale area studies. Readers are referred to the NSIDC's website for more information on this dataset, including documentation and uncertainties. The variability of SC before 1972 is underestimated (Robinson et al., 1993), with the deployment of the AVHRR sensor in 1972 having considerably improved the quality of SC charting. Therefore, we use SC records after 1972 in our study of the interannual variability of snow.

The monthly surface air temperature (SAT) and total precipitation (TPRE) (TS 3.22) data are from the Climatic Research Unit (CRU) at the University of East Anglia (http://dx.doi.org/10.5285/D0E1585D-3417-485F-87AE-4FCECF10A992). This observation-based dataset is on a 0.5° latitude–longitude grid and covers the global land area from 1901 to 2013. To estimate snowfall, the SAT and TPRE are used as inputs to a monthly snow accumulation and melt model; see McCabe and Wolock (2010) for a description of this snow model. Parameters used for the model in this study are the same as those used by McCabe and Wolock (2010). The adoption of these parameters is based on an exhaustive search analysis by Hay et al. (2002).

Atmospheric reanalysis data are extracted from the Japanese 55-year Reanalysis (JRA-55), which is produced and released by the Japan Meteorological Agency (JMA) (Kobayashi et al., 2015). JRA-55 is on a 1.25° latitude–longitude grid and covers the period from 1948 to the present day. Monthly winds at 850 hPa, geopotential height at 500

and 1000 hPa, zonal and meridional water vapor flux, and precipitable water are used. Both SWE and SD from JRA-55 are used to supplement the SC data. Values of SWE and SD have been affected by bugs found in the SD analysis according to a report by the JMA (http://jra.kishou.go.jp/JRA-55/index_en.html#quality). However, the effect is mostly located in coastal areas and is small in scale, thus making it unlikely to affect the current analysis. Surface net shortwave radiation (SWR), net longwave radiation (LWR), latent heat flux (LHF), and sensible heat flux (SHF) are also analyzed in this study. The total heat flux (THF) is defined as sum of these four heat flux terms. The sign convention is that downward heat flux is positive.

## 3. Major patterns of snow variability

Before presenting the major modes of monthly SC variability, we first show the climatological distribution of SC and SAT in autumn. This allows for understanding the relationship between climatological changes of SC and SAT and the snow variability in the context of the climatological distribution.

The climatological mean SC and SAT for the period 1973–2012, for three individual months of autumn, are shown in Fig. 1. The spatial distribution of SC in all three months shows mainly a zonal distribution with a southward decrease (Figs. 1a, c and e). The southward advance of SC from September to November is apparent. The SAT in September and October also shows a zonal distribution, but with a southward increase (Figs. 1b and d). In November, the distribution of SAT is slightly northwest–southeast tilted, with SAT increasing from northeastern Russia towards Southern Europe (Fig. 1f). Overall, the distribution of SC is largely a good match with that of SAT. Therefore, the climatological distribution of autumn SC over northern Eurasia is largely constrained by that of SAT.

An empirical orthogonal function (EOF) analysis is applied to the monthly SC anomalies to obtain the major modes of monthly SC variability. The leading EOF modes and the corresponding principal components (hereafter PC1) for individual calendar months are presented in Fig. 2. The leading modes in September, October, and November explain about 29%, 28%, and 17% of the total SC variability in respective months. The percentage variance explained by PC1 is smaller for November SC than for September and October SC. This may be related to the southward shift of the snow-covered region, which leads to an increase in the large SC variability region such that more EOF modes are needed to explain a similar percentage variance. The corresponding PC1 in September and October features both interannual and interdecadal variations (Figs. 2b and d), and that in November appears to be dominated by interannual variations (Fig. 2f).

In September, the leading mode is characterized by same-sign loading in most regions, with the largest loading located in eastern Siberia to the Russian Far East (Fig. 2a). The large-loading region appears to collocate with the zone of climatological mean SAT varying between −5°C and +5°C (Fig. 1b). In October, the leading mode features same-sign loading over most of northern Eurasia, with the largest loading in a zone extending from Northern Europe to northeast of Lake Baikal (Fig. 2c). The large loading lies in the region with a relatively large north–south gradient of climatological mean SC (Fig. 1c), as well as with climatological mean SAT around zero (Fig. 1d). The leading mode in November displays a very

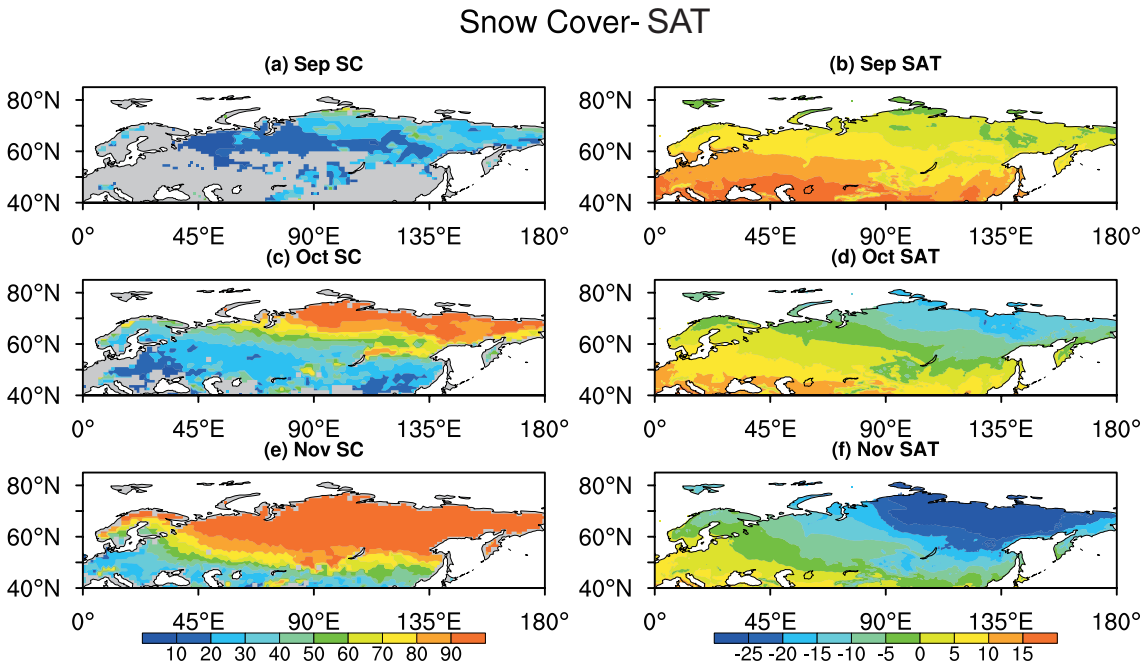


**Fig. 1.** Distribution of climatological monthly mean (a, c, e) SC (units: %) and (b, d, f) SAT (units: °C) in (a, b) September, (c, d) October, and (e, f) November during 1973–2013.

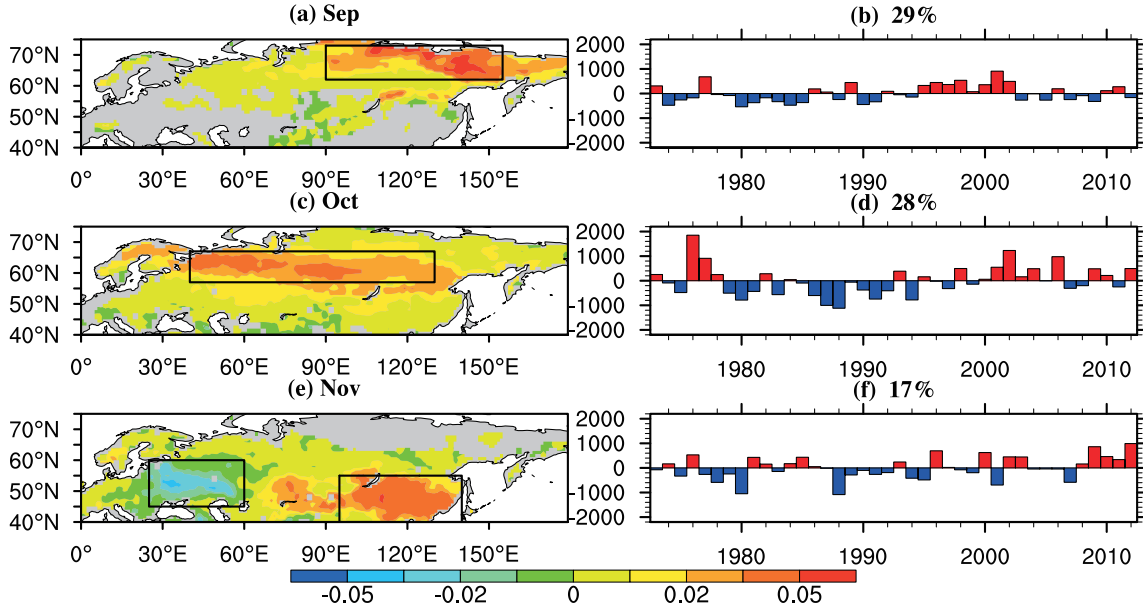


**Fig. 2.** The first EOF mode and corresponding PC of the monthly SC anomaly over northern Eurasia for (a, b) September, (c, d) October, and (e, f) November. The percentage variance explained by each EOF is shown above panels (b, d, f). Units: %. Rectangular boxes denote the domains for calculating the areal averages of the regression coefficients of SAT and heat fluxes, and time series of SAT and snowfall.

different feature compared to that in September and October. A west–east dipole pattern dominates, with the largest loading in Eastern Europe and East Mongolia–Northeast China (Fig. 2e). As in October, these large loadings are located in the regions with a large north–south gradient of climatological mean SC (Fig. 1e) and climatological mean SAT around zero (Fig. 1f). Although the large-loading region varies considerably from month to month, the year-to-year variation of the leading modes in the three months appears to be related. The three PCs yield a correlation coefficient of approximately 0.4 between the neighboring months.

The relationship between the loading and climatological mean distributions indicates that large snow variability tends to occur in the transition zones of climatological mean SC and SAT. Special attention should be paid to these large-loading regions, as snow anomalies in these regions may have substantial effects. Based on the distribution of loading in the major modes, we highlight the region (62°–73°N, 90°–155°E) in September (Fig. 2a), the region (57°–67°N, 40°–130°E) in October (Fig. 2c), and the regions (45°–60°N, 25°–60°E) and (40°–55°N, 95°–140°E) in November (Fig. 2e). These regions are denoted by rectangular boxes in the left-hand panels of Fig. 2. For convenience, the two boxes in November are denoted as the west region and the east region, respectively.

SC variations may be accompanied by changes in snow amount that have implications for the snow-hydrological effect. Here, we examine the SWE and SD anomaly patterns associated with the leading modes of SC variability. Figure 3 shows the distributions of JRA-55 SWE and SD anomalies obtained by regression against the PC1s in the three months, respectively. The anomalies of SWE from NSIDC, with a much shorter temporal coverage (not shown), are mostly consistent with those of SWE from JRA-55, particularly for September and October. Apparently, the patterns of SWE anomalies are rather similar to those of SD anomalies (Figs. 3a, c and e versus Figs. 3b, d and f).

Comparison of Fig. 3 and Figs. 2a, c and e suggests that larger (smaller) SWE and SD accompany higher (lower) SC over the transition zones of climatological mean SC and SAT. However, the largest anomalies in SWE and SD are located in regions of high climatological mean SC and low climatological mean SAT in October and November. The spatial patterns of SWE and SD anomalies are more complicated than those of SC anomalies in both October and November.

## 4. Surface conditions and surface heat fluxes associated with SC variability

Snow and SAT are two closely related variables. On the one hand, SAT is influenced by snow changes, which can modulate the surface energy balance via reflection of SWR and the consumption of heat for snow melting. On the other hand, SAT determines the partitioning of precipitation between rain and snow, and thus makes an important contribution to the amount of snowfall. It also influences the level of snow accumulation. In this section, the SAT, estimated snowfall amount, and surface heat flux anomalies, are analyzed to understand the surface conditions associated with snow changes. Snowfall is estimated using a snow model, as introduced in section 2. These anomalies are obtained by

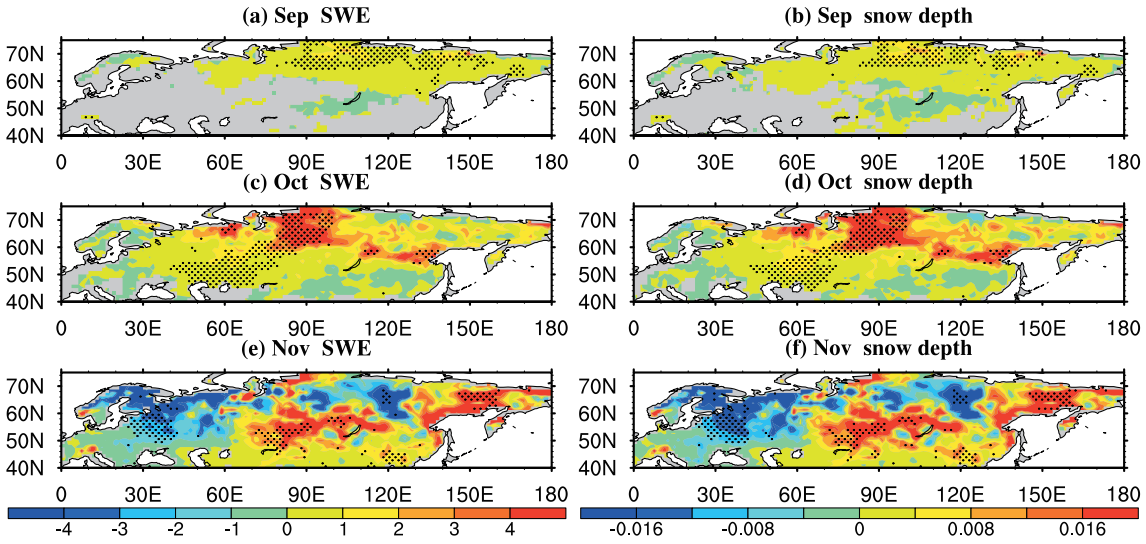


**Fig. 3.** Regression of (a, c, e) SWE (units: kg $m^{-2}$) and (b, d, f) SD (units: m) against the standardized PC of the first EOF mode for September, October and November. Stippling denotes significance at the 5% level.

regression upon the standardized PCs in respective months. The anomalies of SAT and snowfall are presented in Fig. 4.

For September, large-scale surface cooling over northern Eurasia is observed (Figs. 4a). The largest cooling signals are shifted somewhat westwards compared to SC anomalies (Fig. 4a versus Fig. 2a). The distribution of positive snowfall anomalies is rather consistent with that of SC anomalies (Fig. 4b versus Fig. 2a). For October, the zonally extended distribution of negative SAT anomalies is a good match with that of SC anomalies (Fig. 4c versus Fig. 2c). The positive snowfall anomalies are located over the climatological transition zones. However, the largest snowfall anomalies are shifted somewhat southwards. Overall, both lower SAT and above-average snowfall are the causes for larger SC in October. For November, a dipole-like pattern is observed in both SAT and snowfall anomalies, which matches the dipole pattern of SC loading (Figs. 4e and f versus Fig. 2e). Note that the dipoles of SAT and snowfall anomalies display a much larger spatial extent. Overall, lower (higher) SAT and more (less) snowfall are consistent with higher (lower) SC.

Comparison of the snowfall anomaly patterns in Fig. 4 and the SWE anomaly patterns in Fig. 3 reveals some interesting relationships. Around the climatological mean transition zones, both SAT and snowfall seem to contribute to the SWE changes. Lower (higher) SAT and more (less) snowfall favor the accumulation of snow and lead to larger (smaller) SWE. North of the climatological transition zones, the relative contribution of SAT and snowfall to SWE anomalies depends on the month and region. For example, both SAT and snowfall are important in SWE changes over the Arctic areas in September and over western Russia in November. In contrast, lower SAT in October seems to favor the accumulation of snow, and thus larger SWE, in part of the Arctic regions, though there is a lower snowfall amount (Figs. 3c, 4c and 4d). Over northern Siberia in November, decreases in snowfall dictate the smaller SWE (Figs. 3e, 4e and 4f). Similarly, increases in snowfall seem to control the SWE anomalies over the Russian Far East in November. Overall, both SAT and snowfall are important factors for the SWE variability in most areas during autumn.

To quantify the relationships between SC, SAT, and snowfall variations, the correlation coefficients between area-averaged SAT and snowfall anomalies and PC1 for each of the three calendar months are computed. Table 1 summarizes the results. Overall, the correlation coefficient ranges between −0.32 and 0.68, all significant at the 95% confidence level. For regions "September" and "November-West", the SC shows a stronger relationship with snowfall than with SAT. This may indicate the effect of dynamical processes on SWE change through modulating the moisture condition for snowfall. However, as snowfall is associated with SAT in most cases in this study, it is difficult to differentiate the dominant factor.

To understand the thermal condition for snow variability, we perform an analysis of surface heat fluxes. The

**Table 1.** Correlation coefficients between area-averaged SAT, snowfall estimates and the first PC of the EOF mode of the SC anomaly for September, October and November. Domains for averaging are outlined in Fig. 2. The name of the month is used to label the domain if only one domain in that month is used. For two domains in one month, "West" and "East" are used to indicate the relative geophysical location. For regions with negative loadings in the EOF mode, the sign of the correlation coefficient has been reversed to reflect the real relationship. Correlation coefficients significant at the 5% and 1% levels are denoted by double (**) and triple (***) asterisks, respectively.

| Domain | SC PC1-SAT | SC PC1-snowfall |
|---|---|---|
| September | −0.48** | 0.68*** |
| October | −0.50*** | 0.41** |
| November-West | −0.32** | 0.53*** |
| November-East | −0.64*** | 0.60*** |

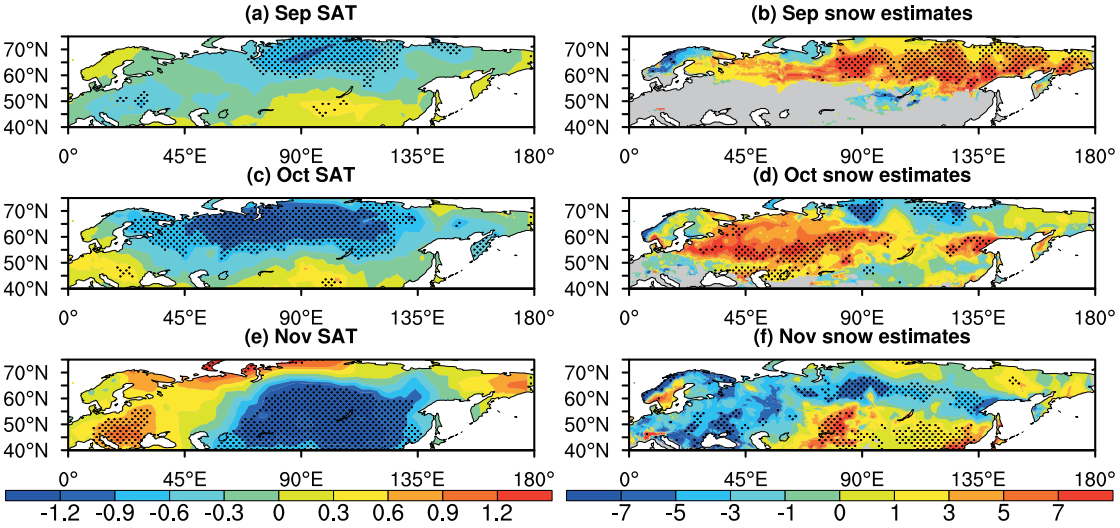


**Fig. 4.** Regression of (a, c, e) SAT (units: °C) and (b, d, f) snowfall (units: mm) against the standardized PC of the first EOF mode for September, October and November. Stippling denotes significance at the 5% level.

surface heat fluxes are determined by both surface and atmospheric states. The former is closely associated with the snow and the latter with the atmospheric processes. Downward components of radiative fluxes are indicative of the effects of atmospheric circulation and atmospheric composition, while upward components of radiative fluxes are associated with ground surface properties. Here, anomalies of SHF, downward SWR (DSWR) and downward LWR (DLWR) are shown in Fig. 5.

The distributions of SHF anomalies bear a rough resemblance to those of SAT anomalies (Figs. 5a, d and g versus Figs. 4a, c and e), except that there are no dipole-like anomalies in November. This resemblance indicates that cooler surface air acts to amplify the land–air temperature difference, and thus leads to more upward SHF. An exception is found in November over Eastern Europe and western Russia, where warmer surface air is accompanied by more upward SHF. The distribution of DSWR anomalies suggests that more DSWR is generally associated with cooler surface air (lower SAT) (Figs. 5b, e and h versus Figs. 4a, c and e). An exception is found in September over the Russian Far East, where less DSWR is co-located with cooler surface air. The anomalies of DLWR are opposite to those of DSWR in most regions (Figs. 5c, f and i versus Figs. 5b, e and h). However, the magnitudes of the DLWR anomalies are notably larger than those of the DSWR and SHF anomalies. Overall, the distributions of the DLWR anomalies, relative to those of the SHF and DSWR anomalies, present a better match to those of the SAT anomalies. This indicates that DLWR is an important factor for surface cooling/warming, and thus for snow changes. As shown below, DLWR anomalies are associated with atmospheric circulation and moisture transport.

To further understand the surface conditions associated with autumn SC variations, areal averages of anomalies of various heat flux terms and SAT are computed. The areal averages are calculated for the highlighted regions in Fig. 2. The results are presented in Fig. 6. The anomalies of DLWR and upward LWR (ULWR) are much larger than those of LHF, SHF and DSWR. Over each region, the DLWR anomaly is of the same sign as the THF and SAT anomaly, while the ULWR anomaly is opposite. Overall, during periods of higher (lower) SC, negative (positive) THF anomalies are observed, mainly due to negative (positive) DLWR anomalies. Thus, DLWR change plays an important role in surface cooling and snow accumulation.

## 5. Atmospheric circulation and moisture transport associated with SC variability

The analyses made in the previous sections indicate that SC variations are associated with anomalies of snowfall, SAT, and surface heat fluxes in climatological transition zones. Large anomalies of these variables are also found in other regions. Although snow feeds back importantly to the surface energy balance and atmospheric circulation, the atmospheric forcing may play an important role in modulating snowfall, surface heat fluxes, and SAT. The changes in SAT can be directly induced by surface heat fluxes as well as by heat advection in the atmosphere. The heat advection effects are assessed in this section. In addition, large-scale atmospheric circulation and moisture transport anomalies are analyzed to explore their relationships with snow variations in terms of DLWR and snowfall anomalies.

Regression patterns of geopotential height at 500 hPa and the thickness between 1000 hPa and 500 hPa are displayed in Fig. 7. In September, the geopotential height anomalies at high latitudes feature an east–west contrast, with positive anomalies over the North Atlantic and negative anomalies over eastern Eurasia (Figs. 7a and b). The negative anomalies over eastern Eurasia provide favorable dynamic conditions for snowfall (Fig. 4b). The atmospheric thickness anomalies indicate a thinner atmospheric column between 1000 hPa and

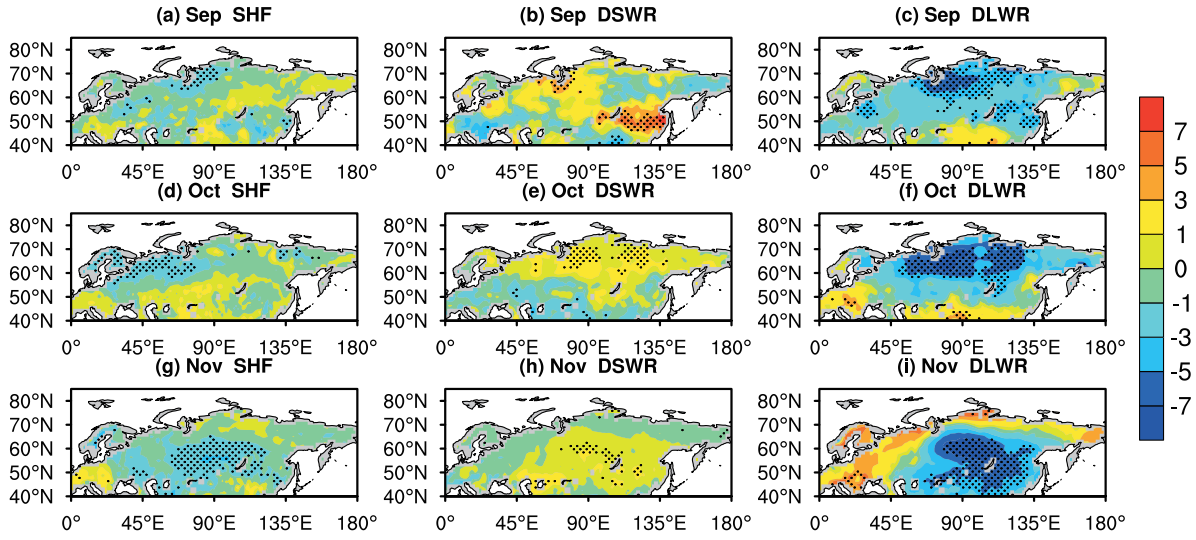


**Fig. 5.** Regression of (a, d, g) SHF (units: W $m^{-2}$), (b, e, h) DSWR (units: W $m^{-2}$), and (c, f, i) DLWR (units: W $m^{-2}$) against the standardized PC of the first EOF mode for September, October and November. Stippling denotes significance at the 5% level.

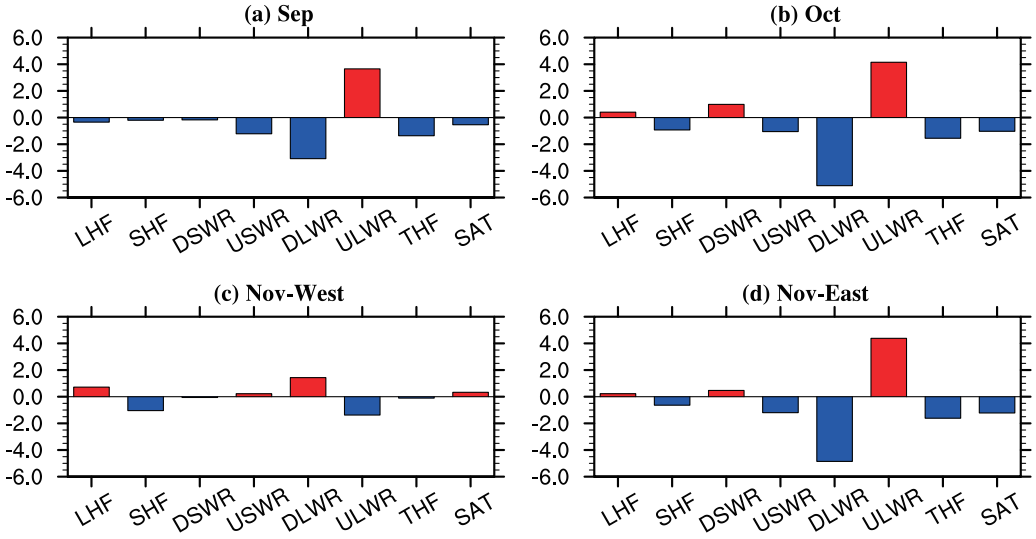


**Fig. 6.** Area-averaged regression coefficients of various surface heat flux terms (units: W $m^{-2}$) and SAT (units: °C) against the standardized PC of the first EOF mode for September, October, and November. Domains for computing the averages are outlined in Fig. 2.

500 hPa, which contributes to the decrease in DLWR. In October, negative geopotential height and thickness anomalies are observed along 45°–65°N (Figs. 7c and d). This reflects a thinner atmospheric column and leads to less DLWR. Increases in geopotential height are observed north of 65°N, indicating a negative phase of the AO. In November, a wave-like pattern is observed over the North Atlantic through Eurasia in both geopotential height and atmospheric thickness anomalies (Figs. 7e and f). The opposite anomalies over the Eurasian land area in both fields resemble the dipole patterns in DLWR, SAT, and snowfall anomalies.

Figure 8 presents the regression of wind field at 850 hPa. For all three calendar months, the wind anomaly patterns are consistent with the geopotential height anomalies at 500 hPa (Figs. 8a–c versus Figs. 7a, c and e), suggesting a barotropic vertical structure of the atmosphere. In September, anomalous northerlies in the Artic regions of central Russia (Fig. 8a) contribute to strong surface cooling there (lower SAT) by bringing colder air from the Arctic Ocean. In October, anomalous easterlies in the sub-Arctic regions (Fig. 8b) are against the climatological westerlies, indicating weaker warm advection from the North Atlantic, and thus leading to surface cooling there. In November, anomalous northeasterlies over Siberia and anomalous southerlies over Western Europe (Fig. 8c) are accompanied by surface cooling and warming, respectively. These results reveal an important contribution

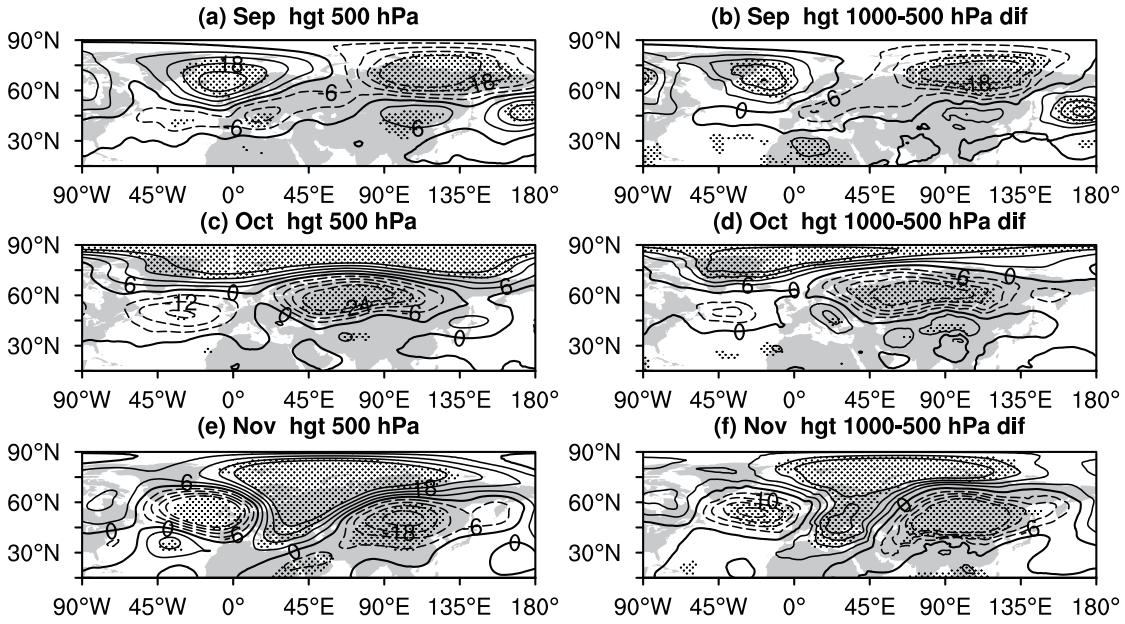


**Fig. 7.** Regression of (a, c, e) geopotential height (units: gpm) and (b, d, f) thickness between 1000 hPa and 500 hPa (units: gpm) against the standardized PC of the first EOF mode for September, October, and November. Solid (Dashed) contours indicate positive (negative) values. Contour intervals are 6 gpm for 500 hPa geopotential height. Contour lines of 0, +/−6, +/−10, +/−14, +/−18 gpm are drawn for panels (b), (d) and (f). Land area is grey. Stippling denotes significance at the 5% level.

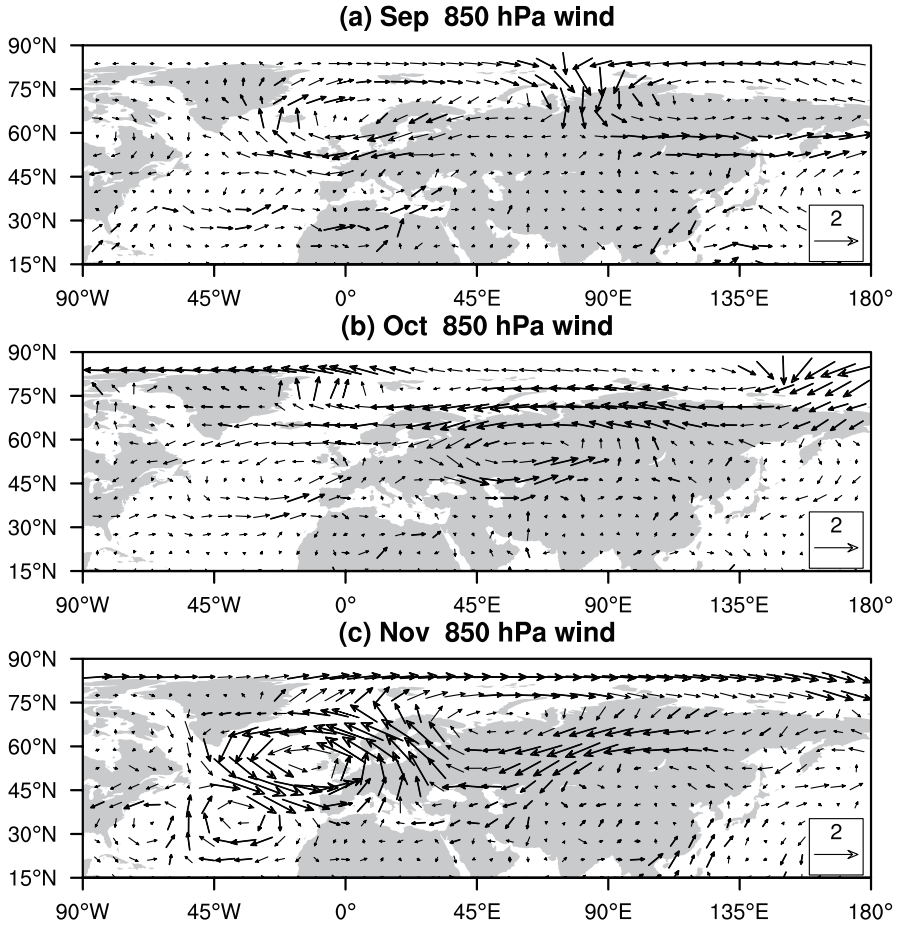


**Fig. 8.** Regression of wind field at 850 hPa (units: m $s^{-1}$) against the standardized PC of the first EOF mode for September, October, and November. Thick vectors denote significance at the 5% level.

of horizontal heat advection to SAT anomalies.

Snowfall events are directly related to the convergence of water vapor flux, which supplies water vapor for snow formation. Figure 9 depicts the regression of water vapor flux anomalies integrated over the entire atmospheric column and their divergence. These regression patterns of water vapor flux anomalies are essentially reminiscent of the lower-level wind anomalies (Fig. 9 versus Fig. 8). As expected, anomalous convergence (divergence) of water vapor flux is overlaid by positive (negative) snowfall anomalies. This confirms an important role of dynamical processes in the snowfall anomalies.

As stated before, DLWR plays an important role in surface heat flux changes. In addition to the atmospheric column cooling, water content in the atmospheric column is also an important factor for the DLWR. The regression of vertically integrated precipitable water anomalies is shown in Fig. 10. The regression patterns of precipitable water are rather similar to those of DLWR, with more (less) precipitable water corresponding to more (less) DLWR. This indicates the impact of atmospheric water content on DLWR change. The reduction in precipitable water is partly associated with enhanced snowfall that acts to remove moisture from the atmospheric column. Another contributing factor is the weakened transport of warm and moist air, and the enhanced transport of cold and dry air. This is indicated by the correspondence between precipitable water and lower-level wind anomalies (Fig. 10 versus Fig. 8). Note that, although the transport of warm and moist air from the south is observed over East Mongolia–Northeast China in November (Fig. 8c), the precipitable water decreases there (Fig. 10c), likely due to increased snowfall (Fig. 4f).

## 6. Summary

The large SC variability over northern Eurasia in autumn tends to occur in the transition zones of climatological monthly mean SC and SAT. With the southward shift of climatological transition zones, the large-loading region in the first mode of SC variations displays a similar southward movement from September to November. Different from September and October, in which the leading mode is dominated by same-sign loading, the leading mode in November features an obvious west–east pattern of contrast.

Analyses show that higher SC is associated with large-scale surface air cooling and increased snowfall. Lower SAT coupled with above-average snowfall leads to larger SC. The variability of SWE is contributed by both SAT and snowfall changes. The relative contribution of SAT and snowfall, however, may vary with region and may depend upon the season.

The changes in SAT and snowfall are associated with atmospheric circulation and radiative processes. The DLWR is a leading term for changes in total surface heat flux, and plays an important role in SAT changes. Anomalous heat advection associated with lower-level wind anomalies also contributes

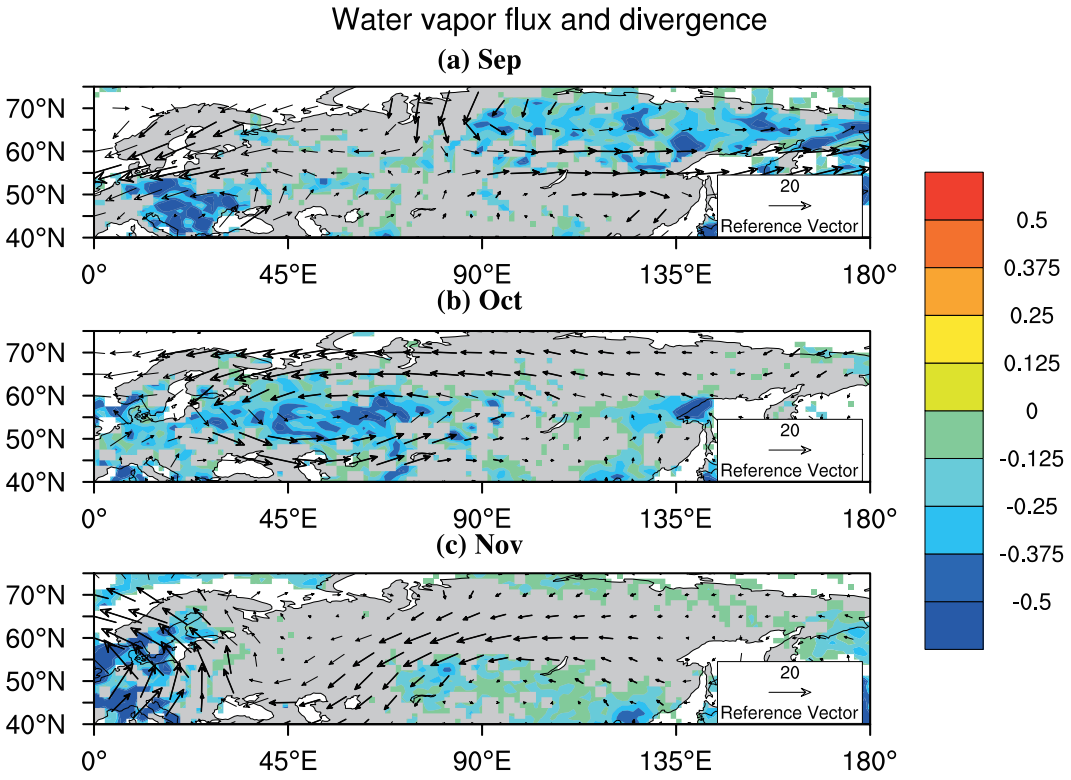


**Fig. 9.** Regression of vertically integrated water vapor flux [vectors; units: kg $m^{-1}$ $s^{-1}$] and its divergence (shading; units: $10^{-5}$ kg $m^{-2}$ $s^{-1}$) against the standardized PC of the first EOF mode for September, October, and November. Thick vectors denote significance at the 5% level.

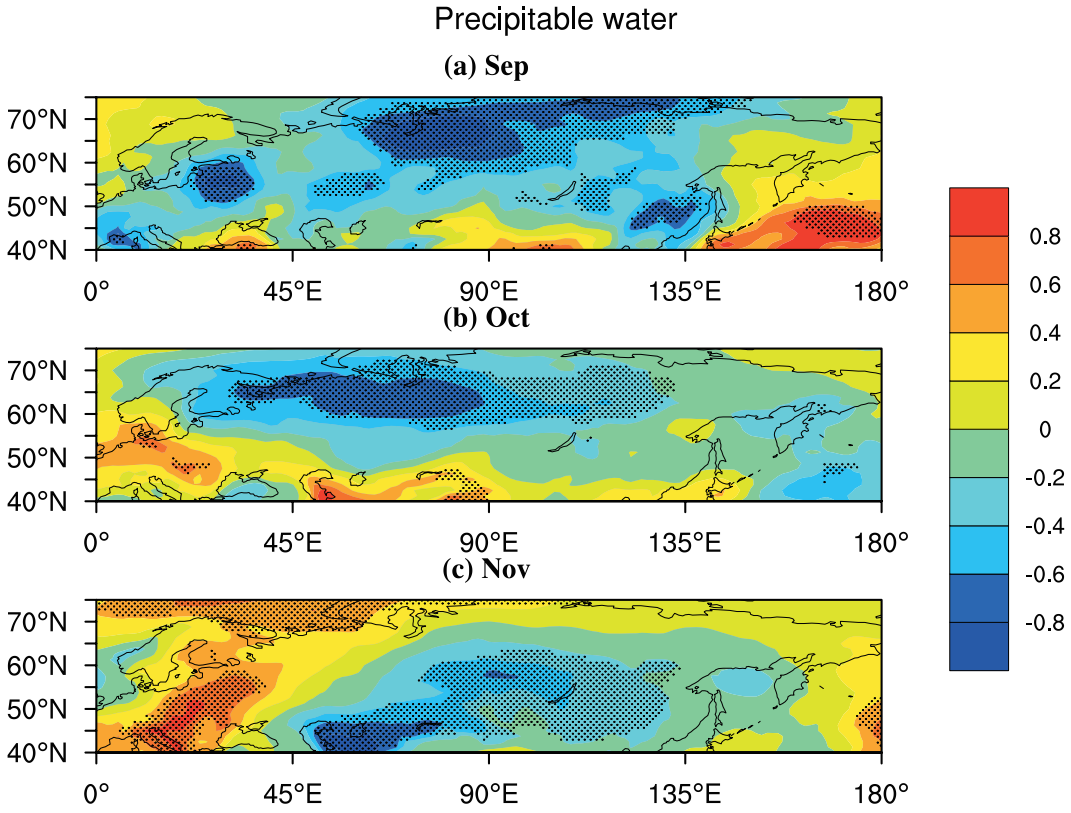


**Fig. 10.** Regression of vertically integrated precipitable water (units: kg $m^{-2}$) against the standardized PC of the first EOF mode for September, October, and November. Stippling denotes significance at the 5% level.

greatly to SAT changes. Anomalous convergence of water vapor flux contributes to enhanced snow fall.

The changes in DLWR are closely associated with those in precipitable water. The decreases in precipitable water observed in both September and October result from a combination of enhanced snowfall and weaker transport of warm moist air. In November, snowfall seems to play a dominant role in the decrease/increase in precipitable water. The DLWR anomalies may also be contributed by the atmospheric column thickness changes.

The present study indicates an important role of atmospheric processes in snow variability in autumn over northern Eurasia. The processes involve moisture convergence–induced snowfall changes, precipitable water–related DLWR changes, and wind-induced heat advection changes. Further studies are needed to understand the coupled features between snow and atmospheric circulation changes. In addition, the year-to-year variability of autumn Eurasian snow and the associated atmospheric circulation has not been found to be driven by external forcing, such as SST.

***Acknowledgements.*** RW is supported by the National Key Basic Research Program of China (Grant No. 2014CB953902) and the National Natural Science Foundation of China (Grant Nos. 41530425, 41275081 and 41475081). We would like to thank the NSIDC, the Met Office Hadley Center, the CRU (University of East Anglia, UK), and the Japan Meteorological Agency, for providing data. We are grateful to Prof. Gabriel LAU for his comments on an earlier version of the manuscript.

## REFERENCES

Allen, R. J., and C. S. Zender, 2011: Forcing of the arctic oscillation by Eurasian snow cover. *J. Climate*, **24**(24), 6528–6539, doi: 10.1175/2011JCLI4157.1.

Bamzai, A. S., and J. Shukla, 1999: Relation between Eurasian snow cover, snow depth, and the Indian summer monsoon: An observational study. *J. Climate*, **12**, 3117–3132, doi: 10.1175/1520-0442(1999)012<3117:RBESCS>2.0.CO;2.

Barnett, T. P., L. Dümenil, U. Schlese, E. Roeckner, and M. Latif, 1989: The effect of Eurasian snow cover on regional and global climate variations. *J. Atmos. Sci.*, **46**(5), 661–686, doi: 10.1175/1520-0469(1989)046<0661:TEOESC>2.0.CO;2.

Barnston, A. G., and R. E. Livezey, 1987: Classification, seasonality and persistence of low-frequency atmospheric circulation patterns. *Mon. Wea. Rev.*, **115**, 1083–1126.

Brodzik, M., and R. Armstrong, 2013: *Northern Hemisphere EASE-Grid 2.0 Weekly Snow Cover and Sea Ice Extent, Version 4*. NASA DAAC at the National Snow and Ice Data Center，Boulder, Colorado, USA.

Chen, L. T., and R. G. Wu, 2000: Interannual and decadal variations of snow cover over Qinghai-Xizang Plateau and their relationships to summer monsoon rainfall in China. *Adv. Atmos. Sci.*, **17**(1), 18–30, doi: 10.1007/s00376-000-0040-7.

Clark, M. P., M. C. Serreze, and D. A. Robinson, 1999: Atmospheric controls on Eurasian snow extent. *International Journal of Climatology*, **19**, 27–40, doi: 10.1002/(SICI)1097-0088(199901)19:1<27::AID-JOC346>3.0.CO;2-N.

Cohen, J., and D. Rind, 1991: The effect of snow cover on the climate. *J. Climate*, **4**(7), 689–706, doi: 10.1175/1520-0442(1991)004<0689:teosco>2.0.co;2.

Cohen, J., and D. Entekhabi, 1999: Eurasian snow cover variability and Northern Hemisphere climate predictability. *Geophys. Res. Lett*., **26**(3), 345–348, doi: 10.1029/1998GL900321.

Cohen, J., and D. Entekhabi, 2001: The influence of snow cover on Northern Hemisphere climate variability. *Atmosphere-Ocean*, **39**(1), 35–53, doi: 10.1080/07055900.2001.9649665.

Cohen, J., J. C. Furtado, J. Jones, M. Barlow, D. Whittleston, and D. Entekhabi, 2014: Linking Siberian snow cover to precursors of stratospheric variability. *J Climate*, **27**, 5422–5432, doi: 10.1175/JCLI-D-13-00779.1.

Dash, S. K., G. P. Singh, M. S. Shekhar, and A. D. Vernekar, 2005: Response of the Indian summer monsoon circulation and rainfall to seasonal snow depth anomaly over Eurasia. *Climate Dyn*., **24**, 1–10, doi: 10.1007/s00382-004-0448-3.

Fasullo, J., 2004: A stratified diagnosis of the Indian monsoon–Eurasian snow cover relationship. *J. Climate*, **17**, 1110–1122, doi: 10.1175/1520-0442(2004)017<1110:ASDOTI>2.0.CO;2.

Gong, G., D. Entekhabi, and J. Cohen, 2003: Modeled Northern Hemisphere winter climate response to realistic Siberian snow anomalies. *J. Climate*, **16**(23), 3917–3931, doi: 10.1175/1520-0442(2003)016<3917:MNHWCR>2.0.CO;2.

Gong, G., D. Entekhabi, and J. Cohen, 2004: Orographic constraints on a modeled Siberian snow tropospheric stratospheric teleconnection pathway. *J. Climate*, **17**(6), 1176–1189, doi: 10.1175/1520-0442(2004)017<1176:OCOAMS>2.0.CO;2.

Gutzler, D. S., and R. D. Rosen, 1992: Interannual variability of wintertime snow cover across the Northern Hemisphere. *J. Climate*, **5**, 1441–1447, doi: 10.1175/1520-0442(1992)005<1441:IVOWSC>2.0.CO;2.

Hay, L. E., M. P. Clark, R. L. Wilby, W. J. Gutowski, G. H. Leavesley, Z. Pan, R. W. Arritt, and E. S. Takle, 2002: Use of regional climate model output for hydrologic simulations. *Journal of Hydrometeorology*, **3**, 571–590.

Henderson, G. R., and D. J. Leathers, 2010: European snow cover extent variability and associations with atmospheric forcings. *International Journal of Climatology*, **30**, 1440–1451, doi: 10.1002/joc.1990.

Henderson, G. R., D. J. Leathers, and B. Hanson, 2013: Circulation response to Eurasian versus north American anomalous snow scenarios in the northern hemisphere with an AGCM coupled to a slab ocean model. *J. Climate*, **26**, 1502–1515, doi: 10.1175/JCLI-D-11-00465.1.

Iijima, Y., K. Masuda, and T. Ohata, 2007: Snow disappearance in Eastern Siberia and its relationship to atmospheric influences. *International Journal of Climatology*, **27**, 169–177, doi: 10.1002/joc.1382.

Kim, Y., K.-Y. Kim, and B.-M. Kim, 2013: Physical mechanisms of European winter snow cover variability and its relationship to the NAO. *Climate Dyn*., **40**, 1657–1669, doi: 10.1007/s00382-012-1365-5.

Kobayashi, S. Y., and Coauthors, 2015: The JRA-55 reanalysis: General specifications and basic characteristics. *J. Meteor. Soc. Japan*, **93**(1), 5–48, doi: 10.2151/jmsj.2015-001.

Kripalani, R. H., S. V. Singh, A. D. Vernekar, and V. Thapliyal, 1996: Empirical study on Nimbus-7 snow mass and Indian summer monsoon rainfall. *International Journal of Climatology*, **16**, 23–24.

Kripalani, R. H., and A. Kulkarni, 1999: Climatology and variability of historical Soviet snow depth data: Some new perspectives in snow–Indian monsoon teleconnections. *Climate Dyn*., **15**, 475–489, doi: 10.1007/s003820050294.

Kripalani, R. H., B.-J. Kim, J.-H. Oh, and S.-E. Moon, 2002: Relationship between Soviet snow and Korean rainfall. *International Journal of Climatology*, **22**, 1313–1325, doi: 10.1002/joc.809.

McCabe, G., and D. Wolock, 2010: Long-term variability in northern hemisphere snow cover and associations with warmer winters. *Climatic Change*, **99**, 141–153.

Morinaga, Y., S.-F. Tian, and M. Shinoda, 2003: Winter snow anomaly and atmospheric circulation in Mongolia. *International Journal of Climatology*, **23**, 1627–1636, doi: 10.1002/joc.961.

Popova, V., 2007: Winter snow depth variability over northern Eurasia in relation to recent atmospheric circulation changes. *International Journal of Climatology*, **27**, 1721–1733, doi: 10.1002/joc.1489.

Robinson, D. A., K. F. Dewey, and R. R. Heim Jr., 1993: Global snow cover monitoring: An update. *Bull. Amer. Meteor. Soc*., **74**, 1689–1696.

Saito, K., J. Cohen, and D. Entekhabi, 2001: Evolution of atmospheric response to early-season Eurasian snow cover anomalies. *Mon. Wea. Rev*., **129**(11), 2746–2760, doi: 10.1175/1520-0493(2001)129<2746:EOARTE>2.0.CO;2.

Saito, K., and J. Cohen, 2003: Correction to "The potential role of snow cover in forcing interannual variability of the major Northern Hemisphere mode". *Geophys. Res. Lett*., **30**, 1302, doi: 10.1029/2002GL016341.

Seager, R., Y. Kushnir, J. Nakamura, M. Ting, and N. Naik, 2010: Northern Hemisphere winter snow anomalies: ENSO, NAO and the winter of 2009/10. *Geophys. Res. Lett*., **37**, L14703, doi: 10.1029/2010GL043830.

Ueda, H., M. Shinoda, and H. Kamahori, 2003: Spring northward retreat of Eurasian snow cover relevant to seasonal and interannual variations of atmospheric circulation. *International Journal of Climatology*, **23**, 615–629, doi: 10.1002/joc.903.

Vicente-Serrano, S. M., M. Grippa, T. Le Toan, and N. Mognard, 2007: Role of atmospheric circulation with respect to the interannual variability in the date of snow cover disappearance over northern latitudes between 1988 and 2003. *J. Geophys. Res*., **112**, D08108, doi: 10.1029/2005JD006571.

Wu, B. Y., K. Yang, and R. H. Zhang, 2009: Eurasian snow cover variability and its association with summer rainfall in China. *Adv. Atmos. Sci*., **26**, 31–44, doi: 10.1007/s00376-009-0031-2.

Wu, R. G., and B. P. Kirtman, 2007: Observed relationship of spring and summer East Asian rainfall with winter and spring Eurasian snow. *J. Climate*., **20**(7), 1285–1304, doi: 10.1175/JCLI4068.1.

Yasunari, T., A. Kitoh, and T. Tokioka, 1991: Local and remote responses to excessive snow mass over Eurasia appearing in the northern spring and summer climate—a study with the MRI·GCM. *J. Meteor. Soc. Japan*, **69**(4), 473–487.

Ye, K. H., R. G. Wu, and Y. Liu, 2015: Interdecadal change of Eurasian snow, surface temperature, and atmospheric circulation in the late 1980s. *J. Geophys. Res*., **120**, 2738–2753, doi: 10.1002/2015JD023148.

Ye, K. H., and N.-C. Lau, 2016: Influences of surface air temperature and atmospheric circulation on winter snow cover variability over Europe. *International Journal of Climatology*,

doi: 10.1002/joc.4868.

Zhang, Y. S., T. Li, and B. Wang, 2004: Decadal change of the spring snow depth over the Tibetan Plateau: The associated circulation and influence on the East Asian summer monsoon. *J. Climate*, **17**, 2780–2793.

Zuo, Z. Y., R. H. Zhang, B. Y. Wu, and X. Y. Rong, 2012: Decadal variability in springtime snow over Eurasia: Relation with circulation and possible influence on springtime rainfall over China. *International Journal of Climatology*, **32**, 1336–1345, doi: 10.1002/joc.2355.